Monocytes shape the neuroprotective and immunomodulatory effects of mesenchymal stromal cell-derived extracellular vesicles

Chen Wang,[1,2] Yiqiao Zhang,[1,2] Tobias Tertel,[3] Yanis Mouloud,[3] Xiaolong Liu,[1,2] Nina Hagemann,[1,2] Ayan Mohamud Yusuf,[1,2] Janine Gronewold,[1,2] Jan-Kolja Strecker,[4,5] Aurel Popa-Wagner,[6] Matthias Mack,[7] Jens Minnerup,[4,5] Matthias Gunzer,[8] Bernd Giebel,[3] Dirk M. Hermann[1,2,6]

[1]Department of Neurology, [2]Center for Translational and Behavioral Neurosciences, and [3]Institute of Transfusion Medicine, University Hospital Essen, University of Duisburg-Essen, Essen, Germany; [4]Department of Neurology, University of Lübeck and University Hospital Schleswig-Holstein, Campus Lübeck, Lübeck, Germany; [5]Department of Neurology, University of Münster, Münster, Germany; [6]Center of Normal and Pathological Ageing, University of Medicine and Pharmacy Craiova, Craiova, Romania; [7]Department of Nephrology, University Hospital Regensburg, Regensburg, Germany; [8]Institute of Experimental Immunology and Imaging, University Hospital Essen, University of Duisburg-Essen, Essen, Germany

Short title: Monocytes shape the neuroprotective effects of MSC-EVs

Words (abstract):	300
Words (total, including title page):	10919
Figures:	6
Supplementary figures:	12
Supplementary tables:	4
Graphical abstract:	1
References:	48

Correspondence: Prof. Dirk M. Hermann, MD, Department of Neurology, University Hospital Essen, University of Duisburg-Essen, Hufelandstr. 55, 45147 Essen, Germany, Email: dirk.hermann@uk-essen.de

Abstract

BACKGROUND: Mesenchymal stromal cell–derived extracellular vesicles (MSC-EVs) exert neuroprotective effects in ischemic stroke largely through immunomodulatory mechanisms. Monocytes are first-line responders to MSC-EVs. Their contribution to MSC-EV-induced neuroprotection remains poorly understood. This study investigated the role of monocytes in shaping neuroprotective responses to MSC-EVs after ischemic stroke.

METHODS: Male C57BL/6J mice were exposed to transient middle cerebral artery occlusion (MCAO). Monocytes were depleted using pharmacological (clodronate liposomes), immunological (anti-CCR2), or genetic (*Mrp8-Cre*$^{+/-}$ *Nr4a1*$^{fl/fl}$) approaches removing total, CCR2^{+}, or Ly6C^{low} monocytes, respectively. In additional cohorts, neutrophils and T cells were simultaneously depleted by anti-Ly6G or anti-CD4/CD8 antibodies. Small EVs from clonally expanded immortalized MSCs were administered intravenously. Neurological deficits, ischemic injury, and immune responses were analyzed up to 72 h post-MCAO. Complementary *ex vivo* studies were performed, in which MSC-EVs were administered to monocyte-depleted or non-depleted peripheral blood mononuclear cells (PBMCs) obtained from acute ischemic stroke patients.

RESULTS: In ischemic mice with an intact monocyte compartment, MSC-EVs reduced neurological deficits, infarct volume, neuronal injury, and brain leukocyte infiltrates. These protective effects were abolished in monocyte-depleted mice, particularly following CCR2^{+} monocyte depletion. Under these conditions, MSC-EV treatment exacerbated neurological deficits, ischemic injury, and leukocyte infiltration, accompanied by neutrophil and T cell expansion and overactivation. Depletion of neutrophils or T cells prevented the EV-induced worsening of stroke outcome in monocyte-deficient mice. Ly6C^{low} monocytes played a crucial role in orchestrating immune responses to MSC-EVs. Their depletion abolished EV-induced neuroprotection. In stroke patient PBMCs, MSC-EVs induced phenotypic reprogramming of monocytes, whereas they promoted CD4^{+} and CD8^{+} T cell activation in the absence of monocytes.

CONCLUSIONS: Monocytes shape the immunomodulatory actions of MSC-EVs. In their absence, MSC-EVs trigger neutrophil and T cell overactivation that worsens stroke

outcome. These findings highlight the importance of monocyte- and T cell-related potency assays for the clinical translation of MSC-EV therapies.
Key words: Ischemic stroke, exosome, antiinflammation, monocyte, non-classical monocyte, neutrophil, T cell.

Introduction

Ischemic stroke remains one of the leading causes of mortality and long-term disability worldwide and limited therapeutic options are available beyond acute reperfusion strategies [1]. Reperfusion therapies (i.e., intravenous thrombolysis and endovascular thrombectomy) considerably improved clinical outcome of ischemic stroke patients in recent years [1]. Despite these benefits, the majority of patients still exhibit long-term disability, and secondary brain injury driven by post-ischemic inflammation plays a significant role in chronic stroke impairments [2]. There is a lack of treatments in the clinical setting able to reverse this inflammatory brain injury. Mesenchymal stromal cell (MSC)-derived small extracellular vesicles (EVs) have emerged as promising candidates for stroke therapy, which bring together the advantages of the pleiotropic mode-of-action of cell therapies with simple handling of EV samples and the lack of malignant transformation risks [3, 4]. In mouse and rat transient middle cerebral artery occlusion (MCAO) models, we and others have shown that intravenously administered MSC-EVs potently promote neurological recovery, reduce infarct volume, and enhance neuronal survival and plasticity [5-8]. Considering their potent actions, MSC-EVs are rapidly approaching clinical proof-of-concept trials [3, 9].

The recovery-promoting effects of MSC-EVs in ischemic stroke models decisively depend on their immunomodulatory properties. In MCAO mice, MSC-EVs with neuroprotective activity effectively reduced the brain infiltration of leukocytes, namely of polymorphonuclear neutrophils, monocytes/macrophages, and lymphocytes [5, 7, 10]. In MCAO mice, in which neutrophils were depleted by a monoclonal anti-Ly6G (lymphocyte antigen-6, locus G) antibody immediately after reperfusion onset, MSC-EV treatment did not reduce neurological deficits and ischemic brain injury [7]. Likewise, MSC-EVs failed to induce vascular remodeling and angiogenesis in mice with delayed neutrophil depletion starting one day after MCAO [10]. These studies underline the importance of immunomodulatory effects for mediating both the neuroprotective and neurorestorative actions of MSC-EVs.

Monocytes are pivotal targets for MSC-EVs in a wide set of inflammatory and degenerative pathologies [11, 12]. When fluorescently labeled MSC-EVs are added to peripheral blood mononuclear cells (PBMCs), they are preferentially internalized by

monocytes and macrophages rather than other leukocytes [13, 14]. MSC-EVs have potent effects on monocytes/macrophages, promoting their polarization from a proinflammatory (M1-like) toward an antiinflammatory (M2-like) phenotype, as shown in mouse myocardial infarction models [15, 16]. Mouse monocyte subsets can be distinguished by their expression of lymphocyte antigen-6 complex, locus C (Ly6C) [17, 18]. While classical Ly6C^{high} monocytes are rapidly recruited to injured tissue closely associated with inflammatory injury where they may convert from M1-like to M2-like cells, non-classical Ly6C^{low} patrolling monocytes contribute to the resolution of inflammation, tissue homeostasis and brain repair [17, 18]. We previously observed that MSC-EVs significantly reduce monocyte accumulation in the ischemic brains of MCAO mice [7, 19]. However, whether monocytes are required for the neuroprotective effects of MSC-EVs has not been investigated in ischemic stroke studies.

To evaluate the role of monocytes in mediating MSC-EV responses, we herein performed transient MCAO studies, in which we depleted monocytes by pharmacological, immunological or genetic tools, and intravenously administered small EVs obtained from clonally expanded immortalized MSCs (ciMSCs), which we generated by a modified human telomerase reverse transcriptase (hTERT) strategy [20]. We have previously shown in a mouse model of neonatal hypoxia–ischemia that small EVs from ciMSCs exert neuroprotective effects comparable to primary MSC-EVs [21, 22]. We now explored whether the neuroprotective effects of ciMSC-EVs (hereafter referred to as MSC-EVs) after MCAO depend on monocytes. To this end, unselective monocyte/macrophage depletion was first used to determine whether monocytes are required for MSC-EV-mediated neuroprotection. Selective depletion of classical Ly6C^{high} monocytes and genetic reduction of non-classical Ly6C^{low} monocytes were subsequently employed to examine the contributions of distinct monocyte populations. Following the observation of exacerbated stroke injury associated with neutrophil and T cell hyperactivation, we further depleted neutrophils or T cells in monocyte-deficient mice to determine whether these leukocyte populations mediate the adverse response to MSC-EVs in the absence of monocytes. Finally, we examined intact and monocyte-depleted PBMCs from patients with acute ischemic stroke to assess whether monocytes

similarly shape MSC-EV-induced immune responses under clinically relevant *ex vivo* conditions.

Materials and Methods

Ethical approval, animal housing, randomization, and blinding

All animal experiments were authorized by the State Office for Consumer Protection and Food North Rhine-Westphalia (Recklinghausen, Germany) and conducted under Directive 2010/63/EU and local institutional guidelines for the care and use of laboratory animals. Reporting followed ARRIVE 2.0 guidelines [23]. Peripheral blood samples were collected from stroke patients which were enrolled in the prospective NOFF-S study (Neutrophils: Origin, Fate & Function Stroke) recruited via the German Research Foundation–funded Collaborative Research Center TRR332 “Neutrophils: origin, fate and function” (https://www.neutrophils.de, subproject C6; https://drks.de/search/en/trial/DRKS00030825). The NOFF-S study was approved by the institutional review board of the University Hospital Essen (approval number 21-10271-BO) and the approval covers both study participation and data publication. Group allocation and experimental assessments were randomized and blinded. A researcher (YZ) not involved in animal studies and histochemical evaluation prepared the vehicle and MSC-EV solutions and assigned them dummy names (i.e., solution A-D). Group information was disclosed only after the study was completed. Mice were housed five per cage under an inverse 12 h light/dark cycle with unrestricted access to water and food. Surgery and behavioral testing were consistently performed during the morning hours.

Statistical planning

Group sizes were planned before experimentation using an online sample-size calculator developed by Robin Ristl (University of Vienna, Austria; https://homepage.univie.ac.at/robin.ristl/samplesize.php). With $\alpha = 0.05$ and a statistical power of 80%, an anticipated difference of 32.5% between group mean value, and a standard deviation equivalent to 25% of the mean value (effect size = 1.3), the

estimated requirement was nine mice per group for behavioral and histochemical analyses [7, 19]. According to our predefined protocol, when no more than two animals were excluded, no replacements were made. If more than two animals were excluded, additional animals were enrolled to compensate for the losses. However, no replacement animals were enrolled in the present study.

MSC culture and characterization

Clonally expanded immortalized MSCs (source 41.5, clone 6) were raised and characterized as we previously described [21, 22]. Briefly, MSCs were maintained in low-glucose Dulbecco's modified Eagle medium (DMEM; Lonza, Cologne, Germany) containing 10% human platelet lysate (produced in house at Institute of Transfusion Medicine) [24], 100 U/mL penicillin-streptomycin-L-glutamine (Thermo Fisher Scientific, Waltham, MA, U.S.A.) and 5 IU/mL heparin (Heparin-Natrium-25000, Ratiopharm, Ulm, Germany). Cultures were passaged at approximately 80% confluence. At passage 3, MSCs were characterized according to International Society of Cell and Gene Therapy (ISCT) criteria [25]. Cell surface phenotypes were analyzed by CytoFLEX flow cytometer with CytExpert 2.3 software (Beckman-Coulter, Krefeld, Germany) measuring surface markers including CD14, CD31, CD34, CD44, CD45, CD73, CD90, CD105, and anti-HLA-DR. MSC osteogenic and adipogenic differentiation was assessed in standard MSC differentiation assays. In the present study, we used the same clonal MSC line as in our recent study [21]. From passage 3 onward, conditioned media were collected at 48 h intervals, removed of cellular debris by centrifugation at 2,000 × g for 15 min, filtered through 0.2 µm filters, and frozen at −20 °C until further processing. Cultures were routinely checked for mycoplasma contamination with the VenorGeM OneStep assay (Minerva Biolabs, Berlin, Germany).

Preparation and characterization of MSC-EV preparations

The MSC-EV preparation used in the present study was identical to our previous studies [21, 22]. EVs were isolated from pooled, thawed conditioned medium using the previously published preparation protocol [7, 19, 21]. In brief, EVs were precipitated from conditioned medium using polyethylene glycol 6000 (PEG), followed by

centrifugation at 1,500 × g for 30 min. Pelleted material was rinsed with 0.9% NaCl and subjected to ultracentrifugation at 110,000 × g for 130 min using a Ti45 rotor (k-factor 133). The final EV pellet was resuspended in 10 mM 4-(2-hydroxyethyl)-1-piperazineethanesulfonic acid (HEPES)/0.9% NaCl (Thermo Fisher Scientific), adjusted to 4×10^7 producer-cell equivalents/mL, and stored at −80 °C. Obtained MSC-EV preparations were characterized using our standard procedures as previously described [7, 19], according to the recommendations of minimal information for studies of extracellular vesicles 2018 and 2023 (MISEV2018 and MISEV2023) [26, 27]. Briefly, particle size and concentration were measured by nanoparticle tracking analysis (Particle Metrix, Meerbusch, Germany), and total protein content was quantified using a bicinchoninic acid assay (Pierce, Rockford, IL, U.S.A.). These measurements and the calculated purity are present in Table S1. Imaging flow cytometry performed previously with the AMNIS ImageStreamX Mark II instrument (Luminex, Seattle, WA, U.S.A.) identified $CD9^+$, $CD63^+$, and $CD81^+$ vesicles in our MSC-EV preparations [21].

Depletion of monocytes, neutrophils, and T cells

For unselective depletion of peripheral monocytes/macrophages, phosphate-buffered saline (PBS) loaded control liposomes or clodronate liposomes (Liposoma, Amsterdam, Netherlands) were injected intravenously 24 h before (50 mg/kg) and 24 and 48 h after (30 mg/kg) middle cerebral artery occlusion (MCAO) according to previously published protocols [28, 29]. Monocyte depletion efficacy by clodronate liposomes was verified by flow cytometry of peripheral blood samples from retro-orbital venous plexus (Figure 1B, C). For depletion of C-C chemokine receptor type 2-positive ($CCR2^+$) monocytes, 20 µg of IgG isotype antibody (rat IgG2b; BE0090; BioXCell, West Lebanon, NH, U.S.A.) or monoclonal anti-CCR2 antibody MC-21 (provided by Matthias Mack) were injected intravenously 12 h before and 24 and 48 h after MCAO [30]. Monocyte depletion efficacy by MC-21 was again verified by flow cytometry of peripheral blood samples from retro-orbital venous plexus (Figure 3B, C). For abolishing non-classical $Ly6C^{low}$ monocytes, *Mrp8-Cre*$^{+/-}$ mice on a C57BL/6J background were crossbred with *Nr4a1*$^{fl/fl}$ mice on a C57BL/6J background (*Nr4a1*^{flox} mice were kindly provided by Pierre Chambon, Institut de Genetique et de Biologie Moleculaire et Cellulaire, Illkirch-

Graffenstaden, France) generating *Mrp8-Cre*$^{+/-}$ *Nr4a1*$^{fl/fl}$ mice (generated by Jens Minnerup). The frequency of circulating Ly6C^{low} monocytes was significantly reduced in *Mrp8-Cre*$^{+/-}$ *Nr4a1*$^{fl/fl}$ mice, verified by flow cytometry of peripheral blood samples from retro-orbital venous plexus (Figure 4B, C). In defined mouse subgroups, neutrophils were depleted by the intraperitoneal injection of 200 µg anti-Ly6G antibody (BE0075-1; BioXCell) 24 h before and 24 h after MCAO [7], or CD4$^+$ and CD8$^+$ T cells were depleted by the intraperitoneal injection of anti-CD4 (BE0119; BioXCell) and anti-CD8 (BE0061; BioXCell) antibodies 24 h before (100 µg each) and 24 h after (50 µg each) MCAO.

Focal cerebral ischemia and MSC-EV treatment

Transient focal ischemia was produced by intraluminal MCAO as we previously described [7, 19]. Briefly, male C57BL/6J mice aged 10–12 weeks (Harlan Laboratories, Darmstadt, Germany) or *Mrp8-Cre*$^{+/-}$ *Nr4a1*$^{fl/fl}$ mice on a C57BL/6J background (provided by Jens Minnerup) were anesthetized with 1.5% isoflurane in 30% O_2/70% N_2O. Buprenorphine (0.1 mg/kg body weight; subcutaneous; Reckitt Benckiser, Slough, U.K.) was administered for analgesia. A feedback-controlled heating device (Fluovac; Harvard apparatus, Holliston, MA, U.S.A.) maintained rectal temperature at 36.5–37 °C. Cerebral perfusion was monitored by laser Doppler flowmetry (Perimed, Stockholm, Sweden) through a probe fixed to the skull over the middle cerebral artery territory. Through a midline neck incision, the left common and external carotid arteries were isolated and ligated and the internal carotid artery temporarily occluded with a clip. A silicon-coated 7-0 monofilament (Doccol Corporation, Sharon, MA, U.S.A.) was inserted through the common carotid artery and advanced to induce MCAO. After 30 min of occlusion, the filament was withdrawn to allow reperfusion. Immediately following reperfusion, mice received a tail-vein injection of either 200 µL saline (as vehicle) or MSC-EV preparations equivalent to 2 × 10^6 cells in 200 µL saline. The incision was then closed. Carprofen (5 mg/kg; intraperitoneal; twice daily; Bayer Vital, Leverkusen, Germany) was administered during the first three days after stroke.

Animal exclusion criteria and dropouts

Initial animal numbers were determined based on an a priori sample size calculation. Animals were excluded according to predefined criteria [5, 7]: (1) surgical duration exceeding 20 min; (2) insufficient reduction in cerebral blood flow (< 75%) following monofilament insertion; (3) lack of reperfusion following monofilament withdrawal; and (4) body weight loss exceeding 20%, respiratory abnormalities (central apnea), or death within three days after MCAO. In the present study, a total of 20 mice were excluded. These animals were not replaced by new animals, since never more than 2 animals were lost in any group. Detailed information on animal allocation, exclusions, and final sample sizes is provided in Table S2.

Analysis of neurological deficits poststroke

Neurological function was assessed 24, 48, and 72 h after MCAO with the Clark scoring [7, 19]. General and focal deficits were scored separately and summed to obtain the total deficit score.

Quantification of infarct size and brain edema

Coronal cryosections (20 µm thick) were sampled at 1-mm rostrocaudal intervals throughout the forebrain and stained with cresyl violet (C5042; Sigma-Aldrich, Taufkirchen, Germany). Infarct areas were quantified in ImageJ (National Institutes of Health, Bethesda, MD, U.S.A.) using the indirect approach to correct for tissue swelling. In brief, the area of healthy ipsilateral tissue was subtracted from the contralateral hemispheric area. Section-level infarct areas were integrated to estimate final infarct volume. Brain edema was expressed as the volume ratio of the ipsilateral to the contralateral hemisphere.

Histological assessment of neuronal injury, leukocyte infiltrates, microvascular thrombosis, and blood-brain barrier permeability

Coronal sections at bregma level, corresponding to the core of the middle cerebral artery territory, were processed for immunostaining. Sections were immersed in 0.1 M PBS supplemented with 0.3% Triton X-100 for membrane permeabilization and then in 10% normal donkey serum (D9663; Sigma-Aldrich) for blocking. Thereafter, sections

were incubated overnight at 4 °C with appropriate primary antibodies, including Alexa Fluor 594-conjugated donkey anti-IgG (1:500; A21203; Thermo Fisher Scientific), rabbit anti-NeuN (neuronal nuclear antigen; 1:500; ab177487; Abcam, Cambridge, U.K.), rat anti-CD31 (1:200; 550274; BD Biosciences, Heidelberg, Germany), goat anti-ICAM-1 (intercellular adhesion molecule-1; 1:600; AF796; R&D, Minneapolis, MN, U.S.A.), rat anti-glycoprotein Ibα (GPIbα) (1:500; M043-0; Emfret Analytics, Eibelstadt, Germany), rabbit anti-collagen-IV (1:500; AB756P; Merck-Millipore, Darmstadt, Germany), rat anti-CD45 (1:200; 05-1416, Merck Millipore), rabbit anti-CD3 (1:100; ab16669; Abcam), or rat anti-Ly6G (1:200; clone 1A8; 127602; Biolegend, San Diego, CA, U.S.A.). After washing, suitable secondary antibodies were applied for 1 h at room temperature. Hoechst 33342 (1:1000; 62249; Thermo Fisher Scientific) was used to label cell nuclei. For NeuN-stained sections, neuronal DNA fragmentation was additionally assessed by terminal deoxynucleotidyl transferase dUTP nick end labeling (TUNEL; 12156792910; Roche Diagnostics, Mannheim, Germany) following the manufacturer's instructions. Stained sections were examined by an inverted Zeiss AxioObserver.Z1 microscope (Carl Zeiss, Jena, Germany). Counts of $NeuN^+/TUNEL^+$ neurons, $CD3^+$ T cells, $Ly6G^+$ neutrophils, and $GPIb\alpha^+$ microthrombi were obtained across the entire ischemic striatum. $CD45^+$ leukocytes were quantified in three defined regions of interest (ROIs; 325 µm × 325 µm each) positioned in the lateral ischemic striatum adjacent to the external capsule. The mean of the three counts was used for analysis. Signal intensities for IgG and ICAM-1/CD31 staining were quantified over the entire ischemic striatum. For IgG measurements, the intensity in the corresponding contralateral, non-ischemic striatum was subtracted as background.

Flow cytometric analysis of blood, spleen, and brain leukocytes

Single-cell suspensions were prepared from blood, spleen, and brain tissue as previously described [7, 19]. At sacrifice, cardiac blood was collected and treated with erythrocyte lysis buffer (420302; BioLegend, CA, U.S.A). Following two washes with 0.1 M PBS, blood leukocytes were pelleted at 500 × g for 5 min at 4 °C and then incubated with the corresponding antibody combinations specified in Table S3 for 30 min at 4 °C. After transcardial perfusion with ice-cold 0.1 M PBS, spleen and brain samples were

collected. Spleens were passed through 70-µm cell strainers (Life Sciences, New York, NY, U.S.A.) while being rinsed with Roswell Park Memorial Institute (RPMI)-1640 medium (Thermo Fisher Scientific) supplemented with 1% HEPES. The resulting suspensions were centrifuged at 500 × g for 5 min at 4 °C, subjected to erythrocyte lysis, and washed twice with 0.1 M PBS. Splenic leukocytes were pelleted again under the same conditions and stained with the antibody panels in Table S3 for 30 min at 4 °C. Brains were separated into ischemic (left) and contralateral (right) hemispheres. To obtain cell suspensions, the ischemic hemispheres were mechanically dissociated through 70-µm cell strainers with continuous rinsing in HEPES-buffered RPMI-1640 medium. After centrifugation at 500 × g for 5 min at room temperature, the pellets were suspended in 37% Percoll (GE Healthcare, Uppsala, Sweden) in 0.1 M PBS and centrifuged at 900 × g for 10 min at room temperature. The myelin-containing layer and Percoll were removed, and the cell pellets were washed twice in 0.1 M PBS. Brain leukocytes were incubated with the antibody mixtures detailed in Table S3 for 30 min at 4 °C. For intracellular staining of regulatory T cells (Tregs), cells were processed with the Transcription Factor Fixation/Permeabilization Buffer Set (424401; BioLegend, CA, U.S.A) according to the manufacturer's instructions. Cell suspensions were analyzed using a CytoFLEX flow cytometer (Beckman-Coulter) and files were evaluated using Kaluza software V2.2 (Beckman-Coulter).

Human peripheral blood mononuclear cell (PBMC) isolation and functional assay

Peripheral blood samples were collected from stroke patients 3–6 days after stroke onset who were enrolled in the NOFF-S study (Neutrophils: Origin, Fate & Function Stroke) recruited via the German Research Foundation–funded Collaborative Research Center TRR332 "Neutrophils: origin, fate and function" (https://www.neutrophils.de, subproject C6; https://drks.de/search/en/trial/DRKS00030825) [31]. Baseline characteristics of the stroke patients are summarized in Table S4. PBMCs were obtained by conventional density-gradient centrifugation as previously reported [32]. Briefly, whole blood collected in ethylenediaminetetraacetic acid (EDTA) Vacutainer tubes was transferred to 50 mL conical tubes and diluted 1:1 with Hanks' Balanced Salt Solution (HBSS; 14175-053; Thermo Fisher Scientific) containing 2 mM EDTA

(AM9260G; Thermo Fisher Scientific). The diluted blood was carefully layered over BioColl separation solution (density 1.077 g/mL; Bio&SELL GmbH, Nuremberg, Germany) and centrifuged at 800 × g for 15 min at 18–22 °C with the brake turned off (deceleration set to 0). The PBMC layer was collected and washed twice with PBS by centrifugation at 300 × g for 8 min. After erythrocyte lysis with lysis buffer (420302; BioLegend, CA, U.S.A) for 5 min followed by washing with PBS, PBMCs were centrifuged at 500 × g for 5 min. For monocyte depletion, PBMCs were subjected to magnetic-activated cell sorting (MACS) using CD14 MicroBeads (130-118-906; Miltenyi Biotec, Bergisch Gladbach, Germany) according to the manufacturer's instructions. A total of 6×10^5 viable intact or monocyte-depleted PBMCs were seeded per well in 96-well U-bottom plates (SARSTEDT, Nümbrecht, Germany) in a final volume of 200 µL. Cells were cultured in RPMI-1640 medium (Thermo Fisher Scientific) supplemented with 100 U/mL penicillin, 100 µg/mL streptomycin (both Thermo Fisher Scientific), and 10% human serum (produced in-house) for 3 days at 37 °C in a humidified atmosphere containing 5% CO_2 in the presence or absence of MSC-EV preparations (5×10^4 cell equivalents in 5 µL). After culturing, cells were harvested and stained with an antibody cocktail containing anti-CD69, anti-CD3, anti-HLA-DR, anti-CD54, anti-CD16, anti-CD14, anti-CD8, and anti-CD4 antibodies (Table S3). Data acquisition was performed using a CytoFLEX flow cytometer with CytExpert 2.3 software and analyzed using Kaluza software (both Beckman-Coulter). For analysis of surface marker expression (CD14, CD16, CD54, and HLA-DR), raw geometric mean fluorescence intensity (MFI) values exported from Kaluza were used.

Animal groups and human cohorts

To investigate the role of monocytes in MSC-EV-mediated neuroprotection and immunomodulation after ischemic stroke, a total of 168 mice across seven independent experimental sets and PBMCs from eight patients with acute ischemic stroke were studied. Animal set 1 examined whether monocytes/macrophages are required for MSC-EV-mediated neuroprotection. Mice were treated with control or clodronate liposomes 24 h before MCAO, followed by vehicle or MSC-EVs after reperfusion. Animals were allocated to four groups: control liposomes + vehicle (n = 10), control

liposomes + MSC-EVs (n = 10), clodronate liposomes + vehicle (n = 9), and clodronate liposomes + MSC-EVs (n = 8). Animal set 2 examined the role of monocytes/macrophages in MSC-EV-mediated immunomodulation by flow cytometry and comprised the same four groups: control liposomes + vehicle (n = 8), control liposomes + MSC-EVs (n = 8), clodronate liposomes + vehicle (n = 7), and clodronate liposomes + MSC-EVs (n = 7). Animal set 3 examined the contribution of $CCR2^{+}$ $Ly6C^{high}$ monocytes. Mice were treated with isotype control or MC-21 antibody before MCAO, followed by vehicle or MSC-EVs after reperfusion, resulting in four groups: isotype control + vehicle (n = 9), isotype control + MSC-EVs (n = 8), MC-21 + vehicle (n = 10), and MC-21 + MSC-EVs (n = 9). Animal set 4 with two groups was used for flow cytometric analysis of $CCR2^{+}$ $Ly6C^{high}$ monocyte-depleted mice treated with vehicle (n = 7) or MSC-EVs (n = 9) after stroke. Animal set 5 comprised two groups and examined the contribution of non-classical $Ly6C^{low}$ monocytes. *Mrp8-Cre*$^{+/-}$ *Nr4a1*$^{fl/fl}$ mice were exposed to MCAO followed by vehicle (n = 9) or MSC-EV treatment (n = 9). Animal set 6 comprised two groups and examined whether neutrophils mediate the adverse response to MSC-EVs following monocyte/macrophage depletion. Monocytes/macrophages and neutrophils were depleted using clodronate liposomes and anti-Ly6G antibody, respectively, and mice subsequently received vehicle (n = 8) or MSC-EVs (n = 8). Animal set 7 comprised two groups and examined the contribution of T cells to the adverse response to MSC-EVs following monocyte/macrophage depletion. Monocytes/macrophages and T cells were depleted using clodronate liposomes and anti-CD4/CD8 antibodies, respectively, followed by vehicle (n = 8) or MSC-EV treatment (n = 7). For the human *ex vivo* experiments, PBMCs were obtained from eight patients with acute ischemic stroke. For each patient, intact and $CD14^{+}$ monocyte-depleted PBMCs were cultured in the presence or absence of MSC-EVs, resulting in four paired experimental conditions: intact PBMCs + vehicle, intact PBMCs + MSC-EVs, monocyte-depleted PBMCs + vehicle, and monocyte-depleted PBMCs + MSC-EVs.

Statistical analysis

Statistical analysis was performed using GraphPad Prism (version 10.4.1; GraphPad Software, San Diego, CA, U.S.A.). Normal distribution was assessed in all datasets

using the Shapiro-Wilk normality test. Normally distributed data were analyzed by one-way ANOVA followed by Tukey's post hoc test (comparisons between ≥ 3 groups) or by unpaired or paired two-tailed Student's t test (comparisons between 2 groups). Non-normally distributed data were evaluated by Kruskal-Wallis test followed by Dunn's multiple comparisons test (comparisons between ≥ 3 groups) or two-tailed Mann-Whitney U test (comparisons between 2 groups). Longitudinal neurological deficits assessed by the Clark score at 24, 48, and 72 h after MCAO were analyzed using two-way repeated-measures ANOVA followed by Tukey's or Šidák's post hoc test for comparisons between groups at each time point. Data were presented as box-and-whisker plots showing the median, interquartile range, minimum and maximum values, and individual data points. $P < 0.05$ was considered statistically significant.

Results

Monocyte/macrophage depletion by clodronate liposomes turns neuroprotection by small MSC-EVs into exacerbation of ischemic brain injury

To explore the effect of monocyte/macrophage depletion on neuroprotective responses to MSC-EVs, we first administered PBS-loaded liposomes (as control) or clodronate liposomes to mice 24 h before transient MCAO (Figure 1A). Flow cytometric analysis of blood samples confirmed efficient depletion of monocytes 24 h after intravenous clodronate liposome administration, including all major monocyte subsets—classical $Ly6C^{high}$ inflammatory, $Ly6C^{int}$ intermediate, and non-classical $Ly6C^{low}$ patrolling monocytes (Figure 1B, C). In addition, clodronate liposomes reduced the frequencies of macrophages and NK cells in the blood, while increasing immature and aged neutrophil, $CD4^+$ T cell, activated $CD8^+$ T cell, and B cell frequencies (Figure S1). Notably, dendritic cell frequencies were not influenced by clodronate liposomes (Figure S1). In MCAO mice treated with PBS-loaded control liposomes, MSC-EV administration immediately after reperfusion significantly reduced neurological deficits over 72 h post-MCAO compared with vehicle, as assessed by the Clark score, which evaluates both general and focal neurological impairments (Figure 1D). Consistently, infarct volume, brain edema, and the density of $TUNEL^+/NeuN^+$ injured neurons were significantly reduced by

MSC-EVs (Figure 1E, F). These findings confirm that the neuroprotective potency of the ciMSC-EVs we used is equivalent to that of primary MSC-EVs administered earlier by our group [5, 7, 10, 19]. Notably, monocyte depletion by clodronate liposomes mimicked the neuroprotective effects of MSC-EVs, significantly reducing neurological deficits, infarct volume, brain edema, and neuronal injury (Figure 1D-F). In contrast, in monocyte-depleted mice, MSC-EV treatment not only failed to induce neuroprotection compared with vehicle treatment, but significantly exacerbated neurological deficits, infarct volume, and neuronal injury (Figure 1D-F) and increased the expression of ICAM-1, a leukocyte adhesion molecule, on cerebral microvessels (Figure 1G). Neither MSC-EVs nor monocyte depletion influenced the density of GPIbα$^+$ microvascular thrombi (Figure S2A) or IgG extravasation, a marker of blood-brain barrier (BBB) permeability (Figure S2B), in the previously ischemic striatum when applied alone or in combination. Together, these data indicate that monocytes are essential mediators of MSC-EV-induced neuroprotection, whereas ischemic injury is exacerbated by MSC-EVs in the absence of monocytes.

Monocyte depletion converts antiinflammatory activity of MSC-EVs into proinflammatory activity

The upregulation of microvascular ICAM-1 expression by MSC-EVs in monocyte-depleted mice (Figure 1G) suggested facilitated immune cell infiltration into the ischemic brain. We therefore investigated the immunomodulatory effects of MSC-EVs in the presence and absence of monocytes. Ischemic brain, blood, and spleen samples were collected at 3 days after MCAO and analyzed by flow cytometry (Figure 2A). In ischemic brains, monocyte depletion alone by clodronate liposomes significantly reduced total brain-infiltrating CD45$^+$ leukocyte numbers, while MSC-EV treatment alone had no overall effect. In contrast, combined monocyte depletion and MSC-EV administration significantly increased brain leukocyte infiltrates (Figure 2B). Analysis of neutrophils within the brain-infiltrating leukocyte population revealed that monocyte depletion and MSC-EV treatment alone significantly reduced brain neutrophil accumulation. Monocyte depletion furthermore decreased the number of activated neutrophils, resting neutrophils, N1-like neutrophils, and N2-like neutrophils in the ischemic brain (Figure

2C, D). Conversely, combined monocyte depletion and MSC-EV treatment tended to increase total neutrophil number ($p = 0.0733$) and significantly increased activated neutrophils in the ischemic brain (Figure 2D). Analysis of lymphocyte subsets showed that monocyte depletion alone significantly reduced post-ischemic brain T cell, activated $CD8^+$ T cell, B cell, and NK cell infiltrates (Figure 2E, F, Figure S3A). In contrast, MSC-EVs significantly increased brain T cell, $CD4^+$ T cell, $CD8^+$ T cell, activated $CD8^+$ T cell, and B cell infiltrates in monocyte-depleted mice (Figure 2F). In the blood, neither monocyte depletion nor MSC-EVs alone significantly influenced leukocyte responses compared with vehicle-treated stroke mice (Figure 2G, Figure S3B). However, combined monocyte depletion and MSC-EV treatment significantly increased total leukocyte number, which comprised T cells, $CD4^+$ T cells, $CD8^+$ T cells, neutrophils, activated neutrophils, aged neutrophils, and immature neutrophils (Figure 2G, Figure S3B). In the spleen, both monocyte depletion alone and combined monocyte depletion and MSC-EV treatment significantly decreased NK cell number (Figure S3C). Flow cytometry of T cell suppressive and exhausted phenotypes revealed that in monocyte-depleted mice treated with MSC-EVs, the number of Tregs, PD-1^+ $CD4^+$ T cells, and PD-1^+ $CD8^+$ T cells was increased in the blood, while PD-1^+ $CD8^+$ T cells were increased in the brain (Figure S4A-C). No significant effects were observed in the spleen (Figure S4D). These findings indicate that monocyte depletion converts the antiinflammatory effects of MSC-EVs into proinflammatory effects, accompanied by the appearance of immunosuppressive and exhausted immune cell phenotypes. Collectively, these data underscore a critical role of monocytes in MSC-EV-induced immunomodulation.

$CCR2^+$ monocytes are indispensable for MSC-EV-induced neuroprotection and antiinflammation after ischemic stroke

Cell depletion by clodronate liposomes is not specific to monocytes/macrophages. Indeed, other phagocytes, such as dendritic cells, have also been reported to be eliminated by clodronate [33]. In addition, clodronate liposomes may induce antiinflammatory effects via myeloid cell, specifically neutrophil stunning [34]. Although we did not observe effects of clodronate liposomes on dendritic cells (Figure S1) or

evidence of neutrophil stunning (Figure S1 and S3), we next specifically depleted monocytes using the anti-CCR2 antibody MC-21 in MCAO mice to elucidate the role of $CCR2^+$ monocyte subsets (Figure 3A). Flow cytometry of blood samples confirmed the depletion of $CCR2^+$ classical monocytes after MC-21 delivery (Figure 3B, C), while frequencies of immature neutrophils and activated $CD4^+$ and $CD8^+$ T cells were increased (Figure S5). In isotype control mice, MSC-EV administration reproducibly reduced neurological deficits, infarct size, and neuronal injury, when administered immediately after reperfusion (Figure 3D-F). $CCR2^+$ monocyte depletion alone reduced neurological deficits, but did not significantly influence infarct volume, brain edema, or neuronal injury (Figure 3D-F). Notably, MSC-EVs again increased neurological deficits, infarct volume, neuronal injury, and ICAM-1 expression in $CCR2^+$ monocyte-depleted mice (Figure 3D-G). Microvascular thrombosis and BBB permeability were unaffected across treatment groups (Figure S6). Flow cytometry revealed that MSC-EVs significantly increased the brain infiltration of leukocytes, particularly neutrophils, activated neutrophils, N1-like neutrophils, and B cells in the ischemic brain of $CCR2^+$ monocyte-depleted mice (Figure 3H, I). Treg frequency (percentage of Tregs in $CD4^+$ T cells) was increased, with a trend toward increased PD-1^+ Tregs ($p = 0.0712$; Figure S7A). MSC-EVs modestly increased Treg frequency in the blood (Figure S7B) and increased aged neutrophils and Treg frequency in the spleen (Figure S7C). Thus, MSC-EV-induced worsening of stroke outcome in $CCR2^+$ monocyte-depleted mice was again associated with exacerbated neutrophil activation, T cell suppression and exhaustion, suggestive of an endogenous protective mechanism activating a compensatory negative feedback loop. These data confirm that $CCR2^+$ monocytes are required for the tuning of inflammatory responses following MSC-EV treatment.

Critical role of non-classical Ly6C^{low} monocytes for post-ischemic neuroprotection and antiinflammation by MSC-EVs

Considering that monocytes were found to regulate immunomodulatory responses, we next investigated the role of non-classical Ly6C^{low} monocyte subsets, which patrol along vascular endothelium and control brain tissue homeostasis [18] using Ly6C^{low} monocyte-deficient *Mrp8-Cre*$^{+/-}$ *Nr4a1*$^{fl/fl}$ mice (Figure 4A). In a steady state of these

mice, circulating Ly6C^{low} monocytes were significantly reduced, whereas Ly6C^{high} and Ly6C^{int} monocyte populations, total macrophage, total neutrophil, and dendritic cell frequencies were unaffected (Figure 4B, C, Figure S8). Moreover, *Mrp8-Cre*$^{+/-}$ *Nr4a1*$^{fl/fl}$ mice exhibited decreased frequencies of M2-like macrophages and resting neutrophils, while immature and aged neutrophil and NK cell frequencies were increased (Figure S8). MSC-EV administration failed to reduce neurological deficits, infarct volume, brain edema, and neuronal injury in Ly6C^{low} monocyte-deficient mice (Figure 4D-F). Although MSC-EVs increased ICAM-1 expression on ischemic microvessels (Figure 4G), the density of brain-invading CD45$^+$ leukocytes, microvascular thrombosis, and BBB permeability remained unchanged (Figure 4H, Figure S9). Peripheral immune analysis (Figure S10A) revealed no significant changes in blood leukocyte composition following MSC-EV treatment in Ly6C^{low} monocyte-deficient mice (Figure S10B), while the numbers of activated CD4$^+$ and CD8$^+$ T cells were increased in the spleen (Figure S10C). Taken together, our data indicate a central role of non-classical Ly6C^{low} monocytes for MSC-EV-induced neuroprotection and immunomodulation after stroke.

MSC-EV-induced exacerbation of ischemic injury is mediated by neutrophils and T cells

Since MSC-EV administration induced neutrophil and T cell expansion and overactivation in monocyte-depleted mice, resulting in the exacerbation of ischemic brain damage, we next investigated whether overactivated neutrophils and/or T cells mediated the exacerbated stroke outcome. In addition to monocyte depletion with clodronate liposomes, we therefore depleted neutrophils or T cells using anti-Ly6G or anti-CD4/CD8 antibody, respectively (Figure 5A). In mice with combined monocyte/neutrophil and combined monocyte/T cell depletion, MSC-EV treatment did not worsen neurological deficits, infarct volume, brain edema, neuronal injury, and ICAM-1 abundance (Figure 5B-E), and did not increase the numbers of brain-infiltrating leukocytes, including neutrophils or T cells (Figure 5F, G). Again, microvascular thrombosis and BBB permeability were not recognizably influenced by MSC-EVs (Figure S11). These findings imply a central role of neutrophil and T cell overactivation in the exacerbated stroke outcome induced by MSC-EVs in monocyte-deficient mice.

MSC-EVs induce functional reprogramming of monocytes in PBMCs from acute ischemic stroke patients

To validate the role of monocytes in mediating MSC-EV-induced immunomodulation across species, we next investigated the effects of MSC-EVs on PBMCs from patients in the acute phase of ischemic stroke. Peripheral blood samples were collected 3–6 days following stroke onset in the prospective NOFF-S cohort [31]. Intact or monocyte-depleted PBMCs were cultured for 3 days in the presence or absence of MSC-EVs, followed by flow cytometry (Figure 6A, B). MSC-EVs significantly increased CD14 and CD54 expression while decreasing CD16 and HLA-DR expression on monocytes (Figure 6C). In line with previous mouse MCAO studies [19], MSC-EVs reduced the frequency of non-classical monocytes (Figure S12A, B), while reducing activated monocyte frequency (Figure 6D). In the absence of monocytes, MSC-EVs increased activated $CD4^+$ and $CD8^+$ T cell frequencies, along with elevated CD54 and HLA-DR expression (Figure 6E, F). Yet, MSC-EVs did not affect the overall frequencies of $CD4^+$ or $CD8^+$ T cells (Figure S12C, D). Together, these findings indicate that MSC-EVs induce phenotypic reprogramming of monocytes and that in the absence of monocytes aberrant T cell activation is induced. Hence, monocytes critically shape the immunomodulatory effects of MSC-EVs in human stroke settings.

Discussion

We herein demonstrate that blood monocytes play a critical role in mediating the neuroprotective and immunomodulatory effects of MSC-EVs in mice exposed to MCAO, a clinically relevant ischemic stroke model. Using pharmacological, immunological, and genetic approaches to delete monocytes, we consistently found that monocyte depletion turned the antiinflammatory effects of MSC-EVs into proinflammatory effects, resulting in the aggravation of ischemic brain damage. Specifically, MSC-EVs increased neutrophil and T cell expansion and activation in the ischemic brain and blood of monocyte-depleted mice, which contributed to the injury-exacerbating effects of MSC-EVs, as shown in studies with dual monocyte/neutrophil and monocyte/T cell depletion. These findings are clinically relevant: MSC-EVs selectively modulated monocyte

differentiation and activation in assays using PBMCs from acute ischemic stroke patients, but increased T cell activation when monocytes were absent. Throughout this study, clonally expanded MSCs were used as EV source, which were immortalized using a modified hTERT strategy [20]. While EVs from primary MSCs exhibit considerable heterogeneity in their immunomodulatory properties due to clonal diversity [7, 10], this heterogeneity is substantially reduced when ciMSCs are used as EV source [12, 20].

In mice with an intact monocyte compartment, MSC-EVs inhibited neutrophil and T cell responses in the ischemic brain of MCAO mice. In monocyte-depleted mice, this inhibitory activity of monocytes was removed, resulting in neutrophil and T cell overactivation in the ischemic brain and blood in response to MSC-EV treatment. MSC-EV-induced worsening of ischemic injury was not detected following combined monocyte/neutrophil or monocyte/T cell depletion. Although the latter experiments did not include direct head-to-head comparisons with animals with monocyte depletion only, these findings collectively support a contribution of neutrophils and T cells to the injury exacerbation by MSC-EVs in monocyte-depleted mice. *In vitro* studies using PBMCs have previously demonstrated immunomodulatory effects of MSC-EVs on monocytes and lymphocytes, including T and B cells [13, 14, 35]. Accumulating evidence indicates that MSC-EV-mediated immunomodulation of T cells occurs indirectly via monocytes [11, 36]. When fluorescently labeled MSC-EVs were added to PBMCs, they were preferentially internalized by monocytes rather than lymphocytes [13, 14]. In *ex vivo* studies using PBMCs obtained from ischemic stroke patients we show that MSC-EVs induce functional monocyte reprogramming reflected by increased CD14 and CD54 expression and reduced CD16 and HLA-DR expression, indicative of a regulatory phenotype that represses T cell activation. It is well established that classical Ly6C^{high} monocytes can adopt reparative roles in ischemic stroke pathologies by promoting M2 macrophage polarization, eliminating necrotic cell debris, and maintaining brain microvasculature stability [17, 37]. That MSC-EVs may induce an antiinflammatory M2-like monocyte phenotype has previously been shown under conditions unrelated to ischemic injury *in vitro* [36]. In that earlier study, the promotion of M2-like monocytes was in line with the differentiation of CD4$^+$ T cells into Tregs [36]. Our results suggest

that MSC-EVs reprogram monocytes toward a regulatory phenotype after stroke that enhances innate immune sensing while limiting adaptive immune responses.

Interestingly, other studies using human PBMCs indicate that the intermediary role of monocytes in EV-mediated regulation of T cell responses may not be restricted to MSC-EVs. Parasitic helminth-derived EVs increased interferon-γ responses in $CD14^+$ monocyte-depleted PBMCs, while suppressing T cell responses in the presence of monocytes [38]. Similarly, glioma stem cell-derived EVs inhibited T cell activation, as indicated by decreased CD25 and CD69 expression, as well as T cell proliferation and Th1 cytokine production in intact PBMCs, but increased T cell proliferation following depletion of $CD14^+$ monocytes [39]. These findings suggest that monocytes may serve not only as major cellular recipients of EVs but also as regulatory intermediaries restraining subsequent T cell responses. In our *ex vivo* assay using PBMCs from acute ischemic stroke patients, monocyte depletion may therefore remove such regulatory pathways. In addition, depletion of a major EV-recipient population may alter the cellular distribution of MSC-EVs and increase their availability to T cells or other immune cells. Increased availability of MSC-EVs to T cells may enhance their exposure to EV-associated adhesion molecules and stress-associated proteins, including collagens, heat shock proteins, and high mobility group box-1 (HMGB1) identified in previous proteomic analyses [40, 41], potentially contributing to the enhanced T cell activation observed in monocyte-depleted PBMCs. Alternatively, other antigen-presenting cells retained in monocyte-depleted PBMC cultures, including B cells and dendritic cells, may respond to MSC-EVs and indirectly contribute to these T cell responses. Because these residual antigen-presenting cells were not selectively depleted or functionally inhibited, our experiments cannot distinguish their potential contribution from direct effects of MSC-EVs on T cells. Further studies are needed to distinguish between these mechanistic possibilities.

In our study, MSC-EVs did not influence cerebral microvascular inflammatory responses, indicated by the adhesion molecule ICAM-1, in ischemic brain tissue of monocyte-competent mice, but increased ICAM-1 levels on ischemic microvessels of monocyte-deficient mice. Interacting with CD11b/CD18 complexes on leukocytes, ICAM-1 mediates the brain tissue infiltration of leukocytes, including neutrophils and T

cells [42]. In our study, ICAM-1 levels increased in response to MSC-EVs in all three monocyte depletion settings, including *Mrp8-Cre*$^{+/-}$ *Nr4a1*$^{fl/fl}$ mice which lacked non-classical Ly6C^{low} patrolling monocytes. Non-classical Ly6C^{low} monocytes control immune responses by patrolling along microvessels [18]. In a microsphere-induced mouse model of cerebral small vessel disease, non-classical Ly6C^{low} monocytes were found to provide neuroprotection and promote microvascular repair in a C-X3-C motif chemokine receptor-1-dependent way [17]. Our results complement these findings by demonstrating that non-classical Ly6C^{low} monocytes constrain microvascular inflammatory responses, preventing the brain entry of leukocytes in MCAO mice. Of note, leukocyte expansion and activation were stronger after combined Ly6C^{high} and Ly6C^{low} monocyte depletion (by clodronate liposomes or anti-CCR2 antibody) than after selective Ly6C^{low} patrolling monocyte deficiency (in *Mrp8-Cre*$^{+/-}$ *Nr4a1*$^{fl/fl}$ mice). Ly6C^{high} inflammatory monocytes can reprogram into Ly6C^{low} antiinflammatory monocytes via Nr4a1 transcription factor activation [18, 43, 44]. Thus, in Ly6C^{low} monocyte-deficient mice, Ly6C^{high} monocyte populations may have compensated for the loss of Ly6C^{low} monocytes, attenuating the impact of Ly6C^{low} monocyte loss on ischemic brain injury. Importantly, MSC-EVs did not enhance stroke outcome in *Mrp8-Cre*$^{+/-}$ *Nr4a1*$^{fl/fl}$ mice. Our results indicate an important role of non-classical Ly6C^{low} monocytes in the immune responses to MSC-EVs in MCAO mice, possibly as a reservoir for non-classical to classical monocyte differentiation. Indeed, MSC-EVs reduced the population of non-classical CD14^{dim} CD16^{+} monocytes in PBMCs of ischemic stroke patients. An overall reduction of non-classical Ly6C^{low} monocytes by MSC-EVs was previously shown by us in the MCAO mouse brain [19]. Hence, immune responses to MSC-EVs are remarkably conserved between mice and humans, which highlights the translational relevance of our results.

The present study has several limitations that warrant further investigation. First, our experiments focused on the acute phase of ischemic stroke, with outcomes evaluated up to 72 h after MCAO. While we have previously shown that neutrophils contribute to the neurorestorative effects of MSC-EVs on vascular remodeling and angiogenesis during the later phase of ischemic stroke [10], whether monocytes similarly mediate the long-term effects of MSC-EVs on functional recovery,

neurovascular remodeling, and brain repair remains to be investigated. In addition, it remains unknown whether the injury-exacerbating effects of MSC-EVs in monocyte-deficient mice persist during subsequent recovery. Although larger infarct volume is generally associated with poorer prognosis [45], the transition from acute ischemic injury to subacute and chronic outcomes can be influenced by immune-cell dynamics shift and/or compensatory mechanisms. Notably, increased frequencies of Tregs in the brain, blood, and spleen were observed in monocyte-deficient mice treated with MSC-EVs after stroke, suggesting the induction of compensatory endogenous immunoregulatory responses. Furthermore, neutrophils and monocytes/macrophages undergo dynamic changes in the phenotypic and functional states across the acute and subacute phases of experimental stroke [46]. Therefore, whether and how these evolving immune cell dynamics and compensatory mechanisms influence long-term functional recovery and tissue remodeling in monocyte-deficient mice treated with MSC-EVs warrants further investigation. Second, although our data identify monocytes as critical intermediaries regulating neutrophil and T cell responses to MSC-EVs, the underlying molecular mechanisms remain unclear. The specific EV cargo responsible for monocyte reprogramming and the monocyte-derived cytokines, metabolites, or other factors regulating subsequent neutrophil and T cell immune responses remain to be identified. Transcriptomic, proteomic, and metabolomic approaches may help reveal these mechanisms. Finally, our genetic experiments suggest an important contribution of Ly6C^{low} monocytes but do not directly resolve the temporal fate or interconversion of Ly6C^{high} and Ly6C^{low} monocyte populations in response to MSC-EVs. Temporally controlled lineage-tracing studies will be required to define their stage-specific contributions to MSC-EV-mediated neuroprotection and immunomodulation. Of note, the experiments on *Mrp8-Cre*$^{+/-}$ *Nr4a1*$^{fl/fl}$ mice did not include concurrent ischemic Cre-negative littermate controls receiving vehicle or MSC-EVs. Although MSC-EV administration failed to improve neurological deficits or histological injury compared with vehicle treatment in *Mrp8-Cre*$^{+/-}$ *Nr4a1*$^{fl/fl}$ mice, we cannot fully exclude potential genotype-associated effects in these studies.

Collectively, our study identifies monocytes as indispensable intermediaries of MSC-EV-mediated immunomodulation repressing neutrophil and T cell activation, thus

enabling the neuroprotective activity of MSC-EVs in ischemic stroke settings. In the forefront of clinical MSC-EV trials, this study emphasizes the need for functional monocyte and T cell assays to evaluate the activity of MSC-EV preparations and rule out side effects or complications [3, 47]. This study advocates thoroughly conducted, possibly personalized activity assays accompanying clinical proof-of-concept trials. Such activity assays will lift cell therapies to the next level. Furthermore, strategies aimed at blocking or depleting the mononuclear phagocyte system to prolong nanoparticle circulation and enhance tissue delivery [48] should be carefully evaluated for MSC-EV applications, since interactions with monocytes/macrophages may be required for their therapeutic efficacy rather than merely a clearance pathway.

Abbreviations

BBB: blood–brain barrier; CCR2: C-C chemokine receptor type 2; ciMSCs: clonally expanded immortalized MSCs; EDTA: ethylenediaminetetraacetic acid; EVs: extracellular vesicles; GPIbα: glycoprotein Ibα; HEPES: 4-(2-hydroxyethyl)-1-piperazineethanesulfonic acid; hTERT: human telomerase reverse transcriptase; ICAM-1: intercellular adhesion molecule-1; ISCT: International Society of Cell and Gene Therapy; Ly6C: lymphocyte antigen 6 complex, locus C; Ly6G: lymphocyte antigen 6 locus G; MCAO: middle cerebral artery occlusion; MISEV2018: Minimal information for studies of extracellular vesicles 2018; MISEV2023: Minimal information for studies of extracellular vesicles 2023; MSC: mesenchymal stromal cell; NeuN: neuronal nuclei antigen; PBMCs: peripheral blood mononuclear cells; PBS: Phosphate-buffered saline; PEG: polyethylene glycol; ROIs: regions of interest; RPMI: Roswell Park Memorial Institute; Tregs: regulatory T cells; TUNEL: terminal deoxynucleotidyl transferase dUTP nick end labeling

Supplemental Material

Figures S1-S12

Tables S1-S4

Acknowledgments

We thank the Imaging Center Essen (IMCES) at the Faculty of Medicine, University of Duisburg-Essen, Germany, for providing imaging support. ChatGPT was used only for language editing and polishing, including the correction of grammatical errors and improvement of clarity and readability.

Funding

This work was supported by the European Union's "National Recovery and Resilience Plan" through the project "Targeting macrophages/monocytes in the aged ischemic brain by pharmacological, genetic, and cell-based tools" (project no. 760058), by German Research Foundation (DFG) grant 514990328, and by the Romanian Executive Agency for Higher Education, Research, Development and Innovation Funding (UEFISCDI) grant PN-IV-P1-PCE-2023-1289 (all to DMH). DMH also received funding via DFG grants 449437943 (C6, within TRR332 "Neutrophils: Origin, fate, and function") and 405358801/428817542 (A4, within FOR2879 "ImmunoStroke"), E.U. ERA-NET NEURON grant 101168752 (SECRET) and German Federal Ministry of Research, Technology, and Space (BMFTR) – NIH - Collaborative Research grant 01GQ2405B (TopoVess).

Authors' contributions

CW and DMH conceived and designed the study. CW, XL, NH, and AMY performed the animal experiments, histological analyses, and data analysis. TT, YM, and BG prepared and characterized MSC-EVs. CW, YZ, and TT performed flow cytometry and analyzed the data. JG provided stroke patient samples and clinical information. CW and TT performed and analyzed the *ex vivo* PBMC assays. MM provided anti-CCR2 antibodies (MC-21) and the corresponding monocyte depletion protocol and interpreted the data. JKS and JM provided the transgenic *Mrp8-Cre*$^{+/-}$ *Nr4a1*$^{fl/fl}$ mice and the clodronate liposome depletion protocol and interpreted the data. CW prepared the figures and drafted the manuscript. All authors critically revised the manuscript and read and approved the final version.

Availability of data and materials

The data that support the findings of this study are available from the corresponding author upon reasonable request.

Competing interests

The authors report no conflict of interest.

References

1. Martin SS, Aday AW, Almarzooq ZI, Anderson CAM, Arora P, Avery CL, et al. 2024 heart disease and stroke statistics: a report of US and global data from the American Heart Association. Circulation. 2024; 149: e347-e913.
2. Iadecola C, Anrather J. The immunology of stroke: from mechanisms to translation. Nat Med. 2011; 17: 796-808.
3. Hermann DM, Peruzzotti-Jametti L, Giebel B, Pluchino S. Extracellular vesicles set the stage for brain plasticity and recovery by multimodal signalling. Brain. 2024; 147: 372-89.
4. Zhang ZG, Buller B, Chopp M. Exosomes — beyond stem cells for restorative therapy in stroke and neurological injury. Nat Rev Neurol. 2019; 15: 193-203.
5. Doeppner TR, Herz J, Gorgens A, Schlechter J, Ludwig AK, Radtke S, et al. Extracellular vesicles improve post-stroke neuroregeneration and prevent postischemic immunosuppression. Stem Cells Transl Med. 2015; 4: 1131-43.
6. Xin H, Li Y, Cui Y, Yang JJ, Zhang ZG, Chopp M. Systemic administration of exosomes released from mesenchymal stromal cells promote functional recovery and neurovascular plasticity after stroke in rats. J Cereb Blood Flow Metab. 2013; 33: 1711-5.
7. Wang C, Börger V, Sardari M, Murke F, Skuljec J, Pul R, et al. Mesenchymal stromal cell-derived small extracellular vesicles induce ischemic neuroprotection by modulating leukocytes and specifically neutrophils. Stroke. 2020; 51: 1825-34.
8. Xin H, Katakowski M, Wang F, Qian JY, Liu XS, Ali MM, et al. MicroRNA cluster miR-17-92 cluster in exosomes enhance neuroplasticity and functional recovery after stroke in rats. Stroke. 2017; 48: 747-53.
9. Manolopoulos A, Yao PJ, Kapogiannis D. Extracellular vesicles: translational research and applications in neurology. Nat Rev Neurol. 2025; 21: 265-82.
10. Gregorius J, Wang C, Stambouli O, Hussner T, Qi Y, Tertel T, et al. Small extracellular vesicles obtained from hypoxic mesenchymal stromal cells have unique characteristics that promote cerebral angiogenesis, brain remodeling and neurological recovery after focal cerebral ischemia in mice. Basic Res Cardiol. 2021; 116: 40.
11. Liu X, Wei Q, Lu L, Cui S, Ma K, Zhang W, et al. Immunomodulatory potential of mesenchymal stem cell-derived extracellular vesicles: targeting immune cells. Front Immunol. 2023; 14: 1094685.
12. Van Hoecke L, Lucci C, Vandenbroucke RE. Mesenchymal stromal cell extracellular vesicles as immune modulators and drug carriers in neurodegenerative disorders. Trends Neurosci. 2025; 48: 919-34.

13. Di Trapani M, Bassi G, Midolo M, Gatti A, Takam Kamga P, Cassaro A, et al. Differential and transferable modulatory effects of mesenchymal stromal cell-derived extracellular vesicles on T, B and NK cell functions. Sci Rep. 2016; 6: 24120.
14. Khare D, Or R, Resnick I, Barkatz C, Almogi-Hazan O, Avni B. Mesenchymal stromal cell-derived exosomes affect mRNA expression and function of B-lymphocytes. Front Immunol. 2018; 9: 3053.
15. Zhao J, Li X, Hu J, Chen F, Qiao S, Sun X, et al. Mesenchymal stromal cell-derived exosomes attenuate myocardial ischaemia-reperfusion injury through miR-182-regulated macrophage polarization. Cardiovasc Res. 2019; 115: 1205-16.
16. Ning Y, Huang P, Chen G, Xiong Y, Gong Z, Wu C, et al. Atorvastatin-pretreated mesenchymal stem cell-derived extracellular vesicles promote cardiac repair after myocardial infarction via shifting macrophage polarization by targeting microRNA-139-3p/Stat1 pathway. BMC Med. 2023; 21: 96.
17. ElAli A, Jean LeBlanc N. The role of monocytes in ischemic stroke pathobiology: new avenues to explore. Front Aging Neurosci. 2016; 8: 29.
18. Lecordier S, Menet R, Allain A-S, ElAli A. Non-classical monocytes promote neurovascular repair in cerebral small vessel disease associated with microinfarctions via CX3CR1. J Cereb Blood Flow Metab. 2023; 43: 1873-90.
19. Wang C, Börger V, Yusuf AM, Tertel T, Stambouli O, Murke F, et al. Postischemic neuroprotection associated with anti-inflammatory effects by mesenchymal stromal cell-derived small extracellular vesicles in aged mice. Stroke. 2022; 53: e14-e8.
20. Brancolini A, Bobbili MR, Pultar M, Mazidi Z, Wieser M, Gamauf J, et al. Immortalization of mesenchymal stromal cells by hTERT does not affect the functional properties of secreted extracellular vesicles. J Biotechnol. 2026; 414: 124-45.
21. Labusek N, Mouloud Y, Köster C, Diesterbeck E, Tertel T, Wiek C, et al. Extracellular vesicles from immortalized mesenchymal stromal cells protect against neonatal hypoxic-ischemic brain injury. Inflamm Regen. 2023; 43: 24.
22. Labusek N, Ghari P, Mouloud Y, Köster C, Diesterbeck E, Hadamitzky M, et al. Hypothermia combined with extracellular vesicles from clonally expanded immortalized mesenchymal stromal cells improves neurodevelopmental impairment in neonatal hypoxic-ischemic brain injury. J Neuroinflammation. 2023; 20: 280.
23. Percie du Sert N, Hurst V, Ahluwalia A, Alam S, Avey MT, Baker M, et al. The ARRIVE guidelines 2.0: updated guidelines for reporting animal research. J Cereb Blood Flow Metab. 2020; 40: 1769-77.
24. Mouloud Y, Staubach S, Stambouli O, Mokhtari S, Kutzner TJ, Zwanziger D, et al. Calcium chloride declotted human platelet lysate promotes the expansion of mesenchymal stromal cells and allows manufacturing of immunomodulatory active extracellular vesicle products. Cytotherapy. 2024; 26: 988-98.
25. Dominici M, Le Blanc K, Mueller I, Slaper-Cortenbach I, Marini FC, Krause DS, et al. Minimal criteria for defining multipotent mesenchymal stromal cells. The International Society for Cellular Therapy position statement. Cytotherapy. 2006; 8: 315-7.
26. Théry C, Witwer KW, Aikawa E, Alcaraz MJ, Anderson JD, Andriantsitohaina R, et al. Minimal information for studies of extracellular vesicles 2018 (MISEV2018): a position statement of the International Society for Extracellular Vesicles and update of the MISEV2014 guidelines. J Extracell Vesicles. 2018; 7: 1535750.

27. Welsh JA, Goberdhan DCI, O'Driscoll L, Buzas EI, Blenkiron C, Bussolati B, et al. Minimal information for studies of extracellular vesicles (MISEV2023): from basic to advanced approaches. J Extracell Vesicles. 2024; 13: e12404.
28. Németh K, Leelahavanichkul A, Yuen PST, Mayer B, Parmelee A, Doi K, et al. Bone marrow stromal cells attenuate sepsis via prostaglandin E2–dependent reprogramming of host macrophages to increase their interleukin-10 production. Nat Med. 2009; 15: 42-9.
29. Schmidt A, Strecker J-K, Hucke S, Bruckmann N-M, Herold M, Mack M, et al. Targeting different monocyte/macrophage subsets has no impact on outcome in experimental stroke. Stroke. 2017; 48: 1061-9.
30. Mildner A, Schmidt H, Nitsche M, Merkler D, Hanisch U-K, Mack M, et al. Microglia in the adult brain arise from Ly-6ChiCCR2+ monocytes only under defined host conditions. Nat Neurosci. 2007; 10: 1544-53.
31. Gronewold J, Hagemann N, Zhang Y, Jung M, Fleischer M, Mohamud Yusuf A, et al. CD177 expression on neutrophils predicts ischemic stroke outcome in humans. Stroke. 2026; 57: 1283-97.
32. Cui C, Schoenfelt KQ, Becker KM, Becker L. Isolation of polymorphonuclear neutrophils and monocytes from a single sample of human peripheral blood. STAR Protoc. 2021; 2: 100845.
33. Ander SE, Davenport BJ, Evans AB, Morrison TE. Systemic clodronate liposome treatment for depletion of blood-contacting phagocytes and investigation of their role in the control of bunyavirus viremia. Methods Mol Biol. 2025; 2893: 285-98.
34. Culemann S, Knab K, Euler M, Wegner A, Garibagaoglu H, Ackermann J, et al. Stunning of neutrophils accounts for the anti-inflammatory effects of clodronate liposomes. J Exp Med. 2023; 220: e20220525.
35. Favaro E, Carpanetto A, Lamorte S, Fusco A, Caorsi C, Deregibus MC, et al. Human mesenchymal stem cell-derived microvesicles modulate T cell response to islet antigen glutamic acid decarboxylase in patients with type 1 diabetes. Diabetologia. 2014; 57: 1664-73.
36. Zhang B, Yin Y, Lai RC, Tan SS, Choo AB, Lim SK. Mesenchymal stem cells secrete immunologically active exosomes. Stem Cells Dev. 2014; 23: 1233-44.
37. Chu HX, Broughton BRS, Ah Kim H, Lee S, Drummond GR, Sobey CG. Evidence that Ly6C(hi) monocytes are protective in acute ischemic stroke by promoting M2 macrophage polarization. Stroke. 2015; 46: 1929-37.
38. Borup A, Sharifpour MF, Rossen LS, Whitehead B, Boysen AT, Olesen R, et al. Helminth extracellular vesicles co-opt host monocytes to drive T cell anergy. J Extracell Vesicles. 2025; 14: e70027.
39. Domenis R, Cesselli D, Toffoletto B, Bourkoula E, Caponnetto F, Manini I, et al. Systemic T cells immunosuppression of glioma stem cell-derived exosomes is mediated by monocytic myeloid-derived suppressor cells. PLoS One. 2017; 12: e0169932.
40. van Balkom BWM, Gremmels H, Giebel B, Lim SK. Proteomic signature of mesenchymal stromal cell-derived small extracellular vesicles. Proteomics. 2019; 19: 1800163.
41. Braga CL, da Silva LR, Santos RT, de Carvalho LRP, Mandacaru SC, de Oliveira Trugilho MR, et al. Proteomics profile of mesenchymal stromal cells and extracellular vesicles in normoxic and hypoxic conditions. Cytotherapy. 2022; 24: 1211-24.

42. Furuya K, Takeda H, Azhar S, McCarron RM, Chen Y, Ruetzler CA, et al. Examination of several potential mechanisms for the negative outcome in a clinical stroke trial of enlimomab, a murine anti-human intercellular adhesion molecule-1 antibody. Stroke. 2001; 32: 2665-74.
43. Hanna RN, Carlin LM, Hubbeling HG, Nackiewicz D, Green AM, Punt JA, et al. The transcription factor NR4A1 (Nur77) controls bone marrow differentiation and the survival of Ly6C− monocytes. Nat Immunol. 2011; 12: 778-85.
44. Heidbreder K, Sommer K, Wiendl M, Müller TM, Atreya I, Hildner K, et al. Nr4a1-dependent non-classical monocytes are important for macrophage-mediated wound healing in the large intestine. Front Immunol. 2023; 13: 1040775.
45. Saunders DE, Clifton AG, Brown MM. Measurement of infarct size using MRI predicts prognosis in middle cerebral artery infarction. Stroke. 1995; 26: 2272-6.
46. Garcia-Bonilla L, Shahanoor Z, Sciortino R, Nazarzoda O, Racchumi G, Iadecola C, et al. Analysis of brain and blood single-cell transcriptomics in acute and subacute phases after experimental stroke. Nat Immunol. 2024; 25: 357-70.
47. Gurriaran-Rodriguez U, Bussolati B, Gimona M, Glebov K, Fujita Y, Marcilla A, et al. From lab to industry: advancing the translational potential of extracellular vesicles through the ISEV Translation, Regulation and Advocacy Committee (ISEV-TRA). J Extracell Vesicles. 2026; 15: e70220.
48. Zelepukin IV, Shevchenko KG, Deyev SM. Rediscovery of mononuclear phagocyte system blockade for nanoparticle drug delivery. Nat Commun. 2024; 15: 4366.

Figures and figure legends:

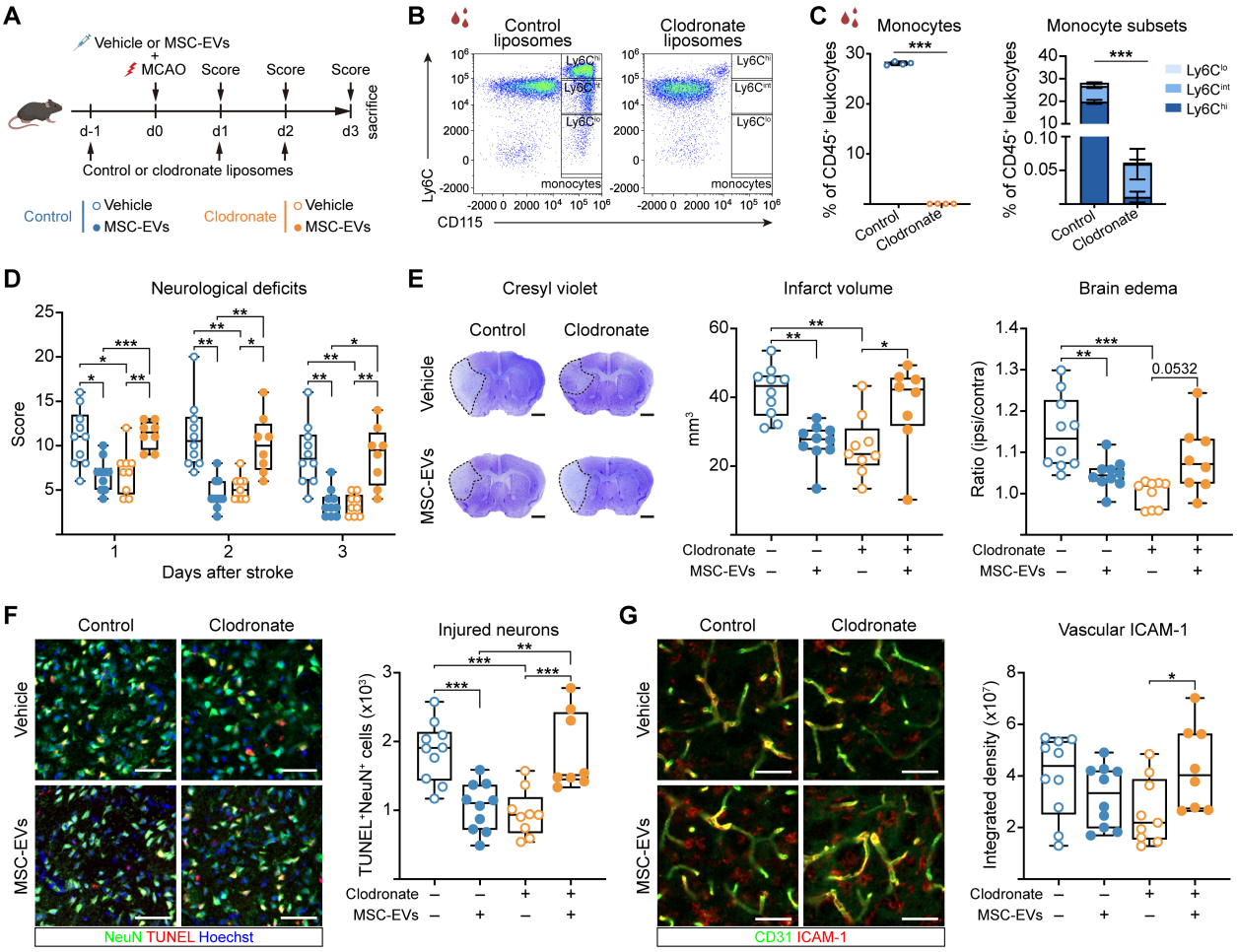

Figure 1. Mesenchymal stromal cell (MSC)-derived extracellular vesicle (EV)-induced neuroprotection turns into exacerbation of ischemic brain injury in monocyte-depleted mice. (**A**) Experimental design: Control or clodronate liposomes were intravenously administered to C57BL/6J wildtype mice 24 h prior to MCAO (50 mg/kg) and 24 and 48 h post-MCAO (30 mg/kg each) for monocyte depletion. Vehicle or small EVs obtained from clonally expanded immortalized MSCs (2 × 10^6 cell equivalents) were intravenously applied immediately after reperfusion. Neurological deficits were evaluated at 24, 48, and 72 h after MCAO using the Clark score, followed by animal sacrifice at 72 h (created with https://BioRender.com). (**B**) Gating strategy for circulating monocytes ($CD11b^+$ $CD115^+$) in the blood classified as classical $Ly6C^{high}$, intermediate $Ly6C^{int}$, and non-classical $Ly6C^{low}$ monocytes. (**C**) Quantification of

monocyte subsets in blood samples of non-ischemic mice 24 h after intravenous administration of control liposomes or clodronate liposomes. (**D**) Neurological deficits using the Clark score assessed at 24, 48, and 72 h post-MCAO. (**E**) Infarct volume and hemisphere brain edema evaluated by cresyl violet staining, (**F**) neuronal injury in the ischemic striatum assessed by terminal deoxynucleotidyl transferase dUTP nick end labeling (TUNEL)/NeuN labeling, and (**G**) ICAM-1 expression on $CD31^+$ microvessels in the ischemic striatum at 72 h post-MCAO. Representative cresyl violet stainings (in **E**) and immunohistochemistry images (in (**F, G**)) are shown. Data were evaluated by unpaired *t* test (in (**C**)), two-way repeated-measures ANOVA followed by Tukey's post hoc test (in (**D**)), or one-way ANOVA followed by Tukey's post hoc test (in (**E-G**)). *$p < 0.05$, **$p < 0.01$, ***$p < 0.001$ ($n = 4$ mice/group (in (**C**)), $n = 8–10$ mice/group (in (**D-G**)). Scale bars: 1 mm (in (**E**)), 50 µm (in (**F, G**)).

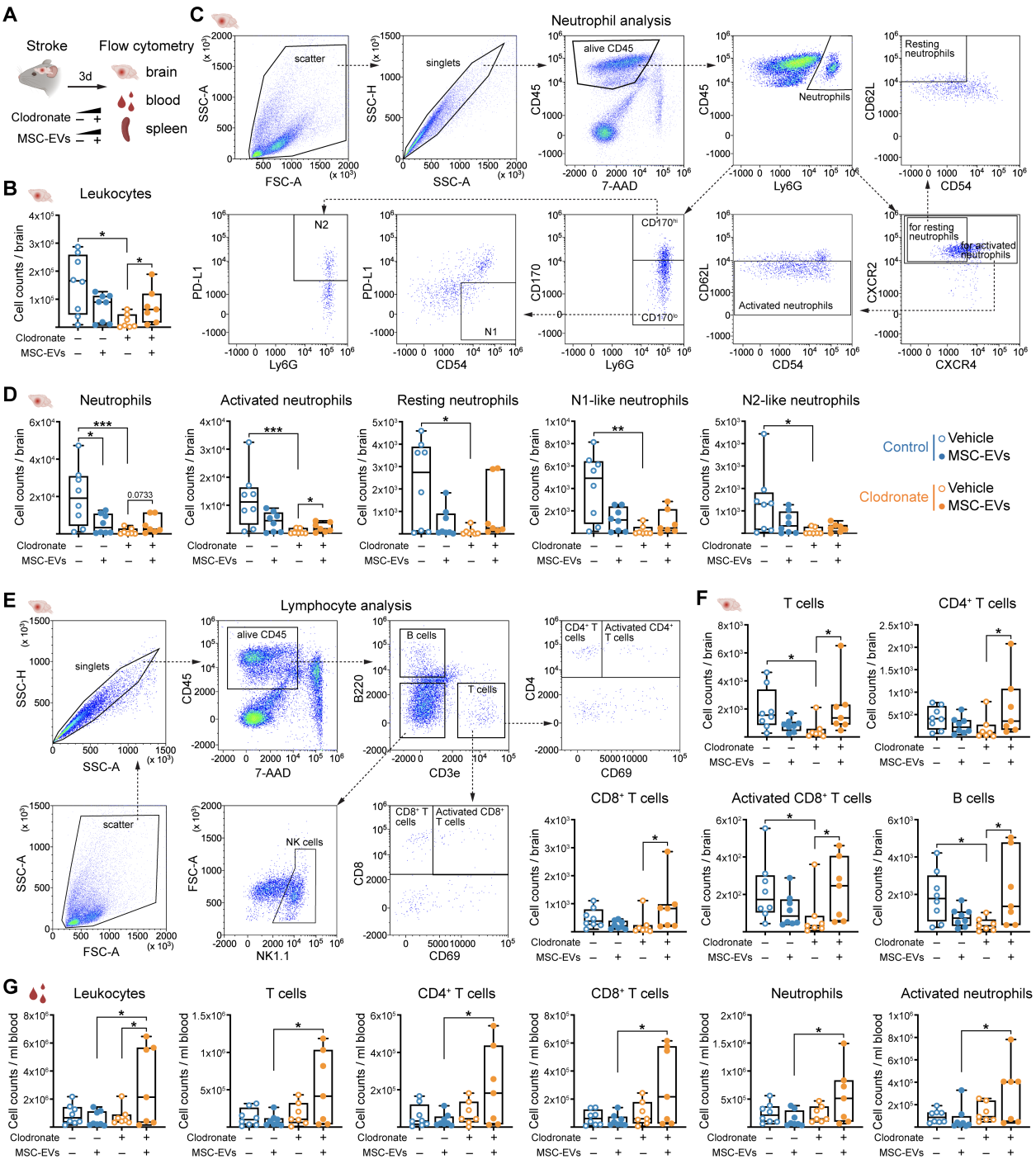

Figure 2. MSC-EVs augment post-ischemic cerebral inflammatory responses and peripheral immune activation in monocyte-depleted mice. (**A**) Experimental design: Mice were intravenously treated with control or clodronate liposomes for monocyte depletion (see Figure 1A), and vehicle or MSC-EVs (2×10^6 cell equivalents) were intravenously applied immediately after MCAO. Ischemic brain, blood, and spleen

samples were collected at 72 h after MCAO for flow cytometry (created with https://BioRender.com). (**B**) Quantification of total $CD45^+$ leukocytes in ischemic brain. (**C**) Gating strategy for analysis of neutrophils within brain-invading leukocytes. (**D**) Quantification of neutrophil subsets in ischemic brain, including neutrophils ($Ly6G^+$), activated neutrophils ($Ly6G^+$ $CXCR2^+$ $CD62L^{low}$), resting neutrophils ($Ly6G^+$ $CXCR2^+$ $CXCR4^-$ $CD62L^{high}$ $CD54^{low}$), N1-like neutrophils ($Ly6G^+$ $CD170^{low}$ $CD54^+$ PD-$L1^-$), and N2-like neutrophils ($Ly6G^+$ $CD170^{high}$ PD-$L1^+$). (**E**) Gating strategy for lymphocyte subsets. (**F**) Quantification of lymphocyte subsets in ischemic brain, including T cells ($CD3e^+$), $CD4^+$ T cells ($CD3e^+$ $CD4^+$), $CD8^+$ T cells ($CD3e^+$ $CD8^+$), activated $CD8^+$ T cells ($CD3e^+$ $CD8^+$ $CD69^+$), and B cells ($CD3e^-$ $B220^+$). (**G**) Quantification of leukocyte subsets in peripheral blood, including total $CD45^+$ leukocytes, T cells, $CD4^+$ T cells, $CD8^+$ T cells, neutrophils, and activated neutrophils. Data were compared by Kruskal-Wallis test with Dunn's post hoc test or one-way ANOVA with Tukey's post hoc test. *$p < 0.05$, **$p < 0.01$, ***$p < 0.001$ ($n = 7–8$ mice/group).

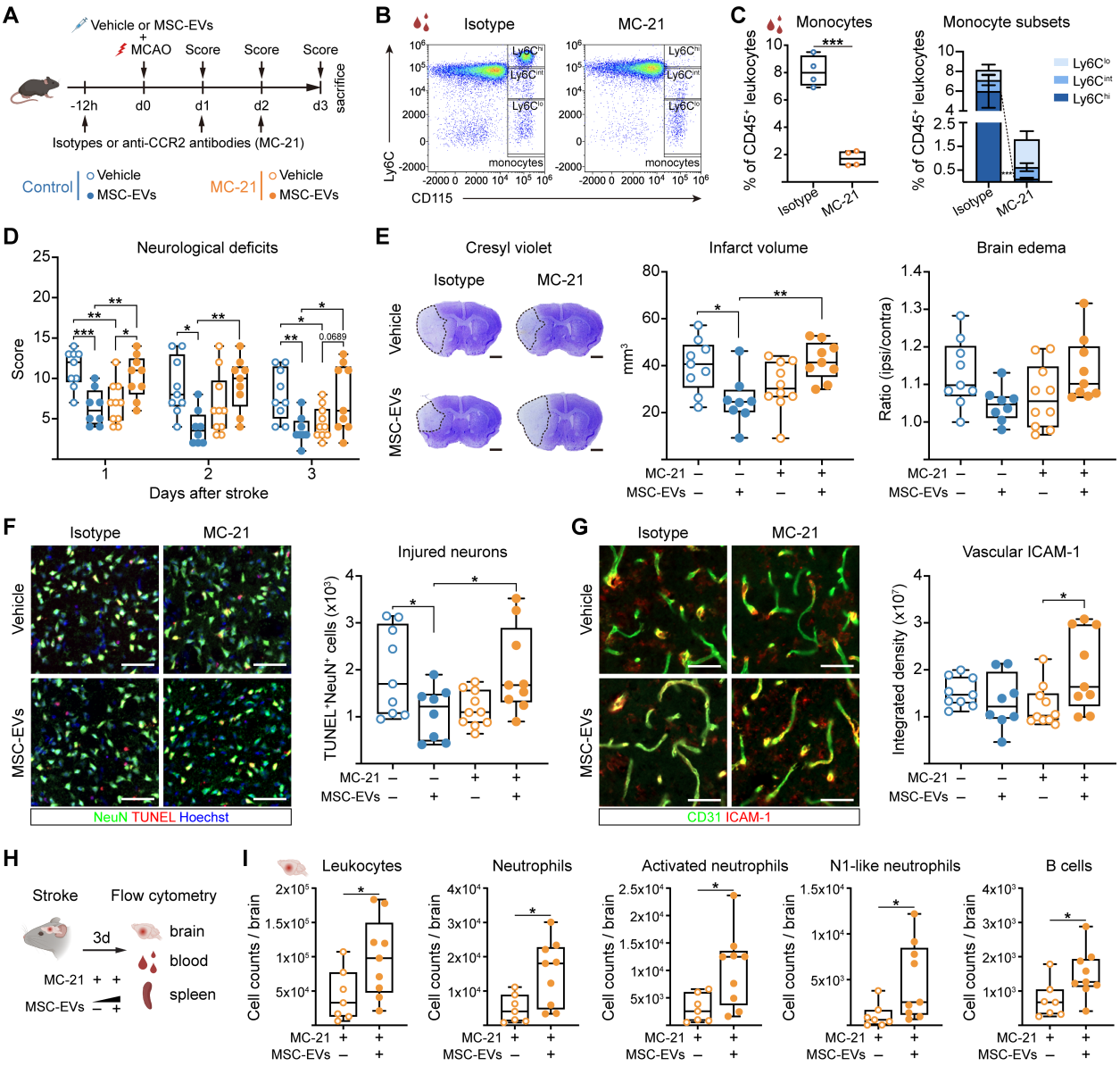

Figure 3. MSC-EVs aggravate ischemic stroke outcome and increase brain inflammatory responses in mice exhibiting CCR2⁺ monocyte depletion. (**A**) Experimental design: Isotype control antibody or monoclonal anti-CCR2 antibody (MC-21) was intravenously injected 12 h prior to MCAO and 24 and 48 h after MCAO (20 µg each) for monocyte depletion. Vehicle or MSC-EVs (2×10^6 cell equivalents) were intravenously administered immediately after reperfusion. Neurological deficits were evaluated at 24, 48, and 72 h. Animals were sacrificed at 72 h post-MCAO for histochemical analyses (created with https://BioRender.com). (**B**) Gating strategy for circulating monocytes ($CD11b^+$ $CD115^+$) in blood classified as classical $Ly6C^{high}$,

intermediate Ly6C^{int}, and non-classical Ly6C^{low} monocytes. (**C**) Quantification of monocyte subsets in non-ischemic mice 12 h after the administration of isotype control or MC-21 antibody. (**D**) Neurological deficits assessed at 24, 48, and 72 h after MCAO using the Clark score. (**E**) Infarct volume and brain edema evaluated by cresyl violet staining, (**F**) neuronal injury in the ischemic striatum assessed by TUNEL/NeuN immunolabeling, and (**G**) ICAM-1 expression on CD31^{+} microvessels in the ischemic striatum at 72 h post-MCAO. (**H**) Experimental design: Anti-CCR2 antibody (MC-21) was injected for monocyte depletion (as above), and vehicle or MSC-EVs (as above) were intravenously applied immediately after reperfusion. Ischemic brain, blood, and spleen samples were harvested at 72 h post-MCAO for flow cytometry (created with https://BioRender.com). (**I**) Quantification of leukocyte subsets in ischemic brain, including total leukocytes, neutrophils, activated neutrophils, N1-like neutrophils, and B cells. Representative cresyl violet stainings (in (**E**)) and immunohistochemistry images (in (**F**, **G**)) are shown. Data were compared by unpaired *t* test (in (**C**, **I**)), two-way repeated-measures ANOVA followed by Tukey's post hoc test (in (**D**)), or one-way ANOVA followed by Tukey's post hoc test (in (**E**-**G**)). *$p < 0.05$, **$p < 0.01$, ***$p < 0.001$ ($n = 4$ mice/group (in (**C**)), $n = 8–10$ mice/group (in (**D**-**G**)), $n = 7–9$ mice/group (in (**I**)). Scale bars: 1 mm (in (**E**)), 50 µm (in (**F**, **G**)).

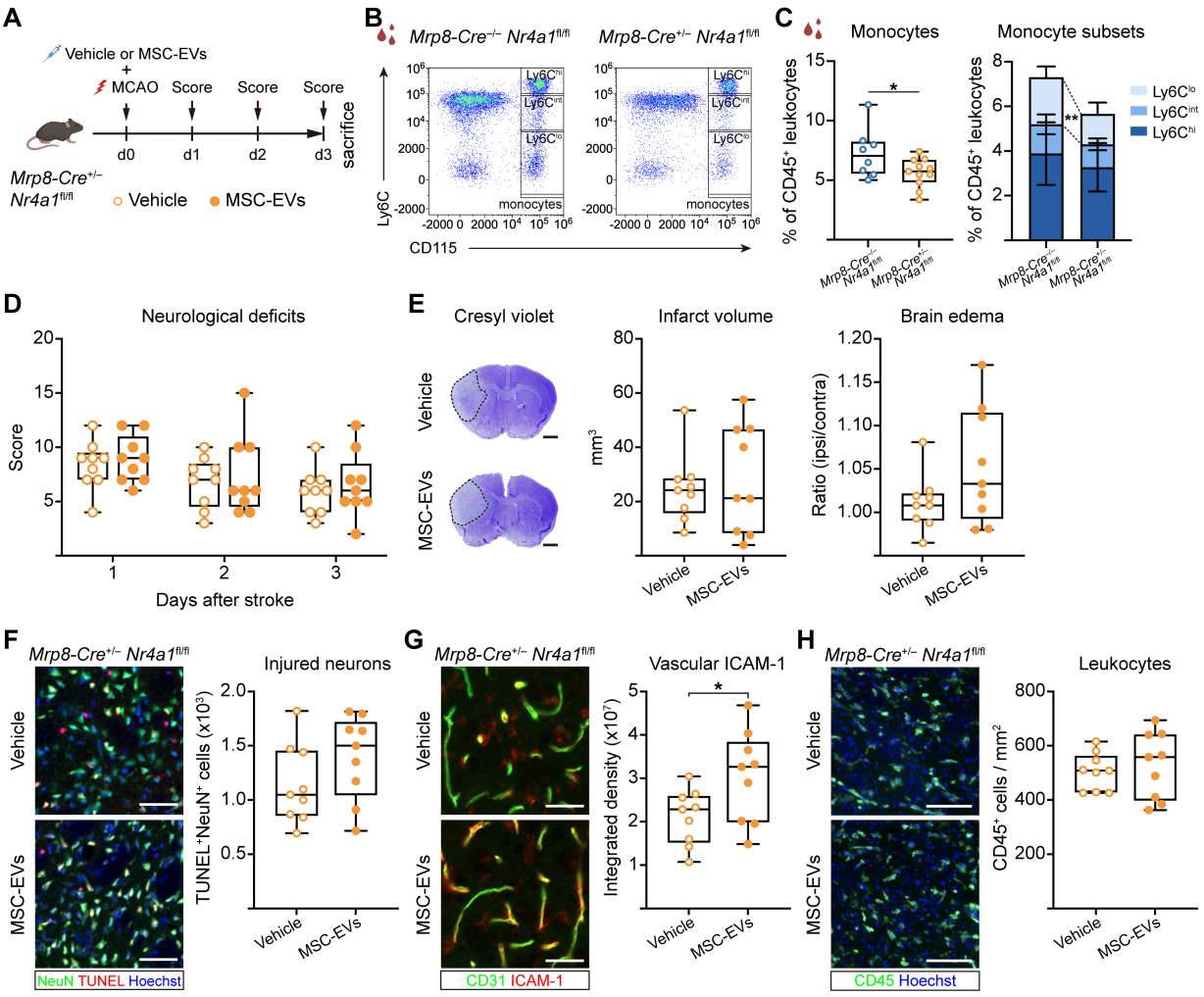

Figure 4. MSC-EVs fail to protect against ischemic injury and reduce brain inflammatory responses in mice deficient in non-classical Ly6C^{low} monocytes. (**A**) Experimental design: Non-classical Ly6C^{low} monocyte deficiency was assessed in *Mrp8-Cre*$^{+/–}$ *Nr4a1*$^{fl/fl}$ mice relative to Cre-negative controls under non-ischemic conditions. Following MCAO, vehicle or MSC-EVs (2 × 10^6 cell equivalents) were intravenously administered immediately after reperfusion, followed by animal sacrifice at 72 h post-MCAO (created with https://BioRender.com). (**B**) Gating strategy for circulating monocytes (CD11b$^+$ CD115$^+$) and (**C**) quantification of monocytes and monocyte subsets in the blood of non-ischemic *Mrp8-Cre*$^{–/–}$ *Nr4a1*$^{fl/fl}$ control and *Mrp8-Cre*$^{+/–}$ *Nr4a1*$^{fl/fl}$ mice. (**D**) Neurological deficits evaluated using the Clark score at 24, 48, and 72 h post-MCAO. (**E**) Infarct volume and brain edema evaluated by cresyl violet staining, (**F**) neuronal injury in the ischemic striatum assessed by TUNEL/NeuN immunolabeling, (**G**) ICAM-1 expression on CD31$^+$ microvessels in the ischemic

striatum and (**H**) density of brain-infiltrating CD45$^+$ leukocytes in the ischemic striatum at 72 h post-MCAO. Representative cresyl violet stainings (in (**E**)) and immunohistochemistry images (in (**F-H**)) are shown. Data were compared by two-way repeated-measures ANOVA followed by Šidák's post hoc test (in (**D**)) or unpaired *t* test (in (**E-H**)). *p < 0.05, **p < 0.01 (n = 9 mice/group). Scale bars: 1 mm (in (**E**)), 50 µm (in (**F**, **G**)), 100 µm (in (**H**)).

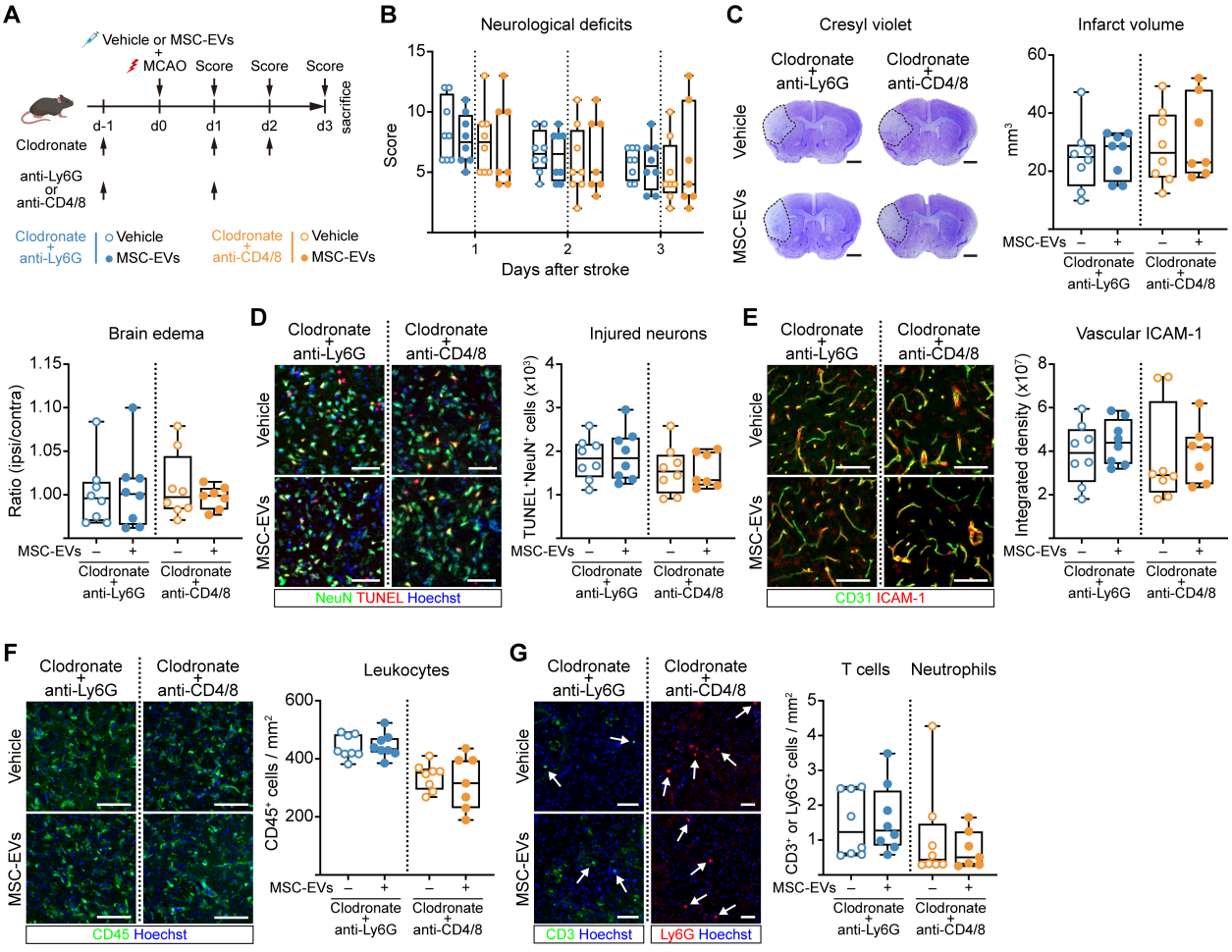

Figure 5. MSC-EV-induced exacerbation of stroke outcome in monocyte-depleted mice is abolished by additional neutrophil or T cell depletion. (**A**) Experimental design: In mice with clodronate liposome-induced monocyte depletion (as above, see Figure 1A), polymorphonuclear neutrophils or T cells were depleted by anti-Ly6G or anti-CD4/CD8 antibody administration 24 h before and 24 h after MCAO. Vehicle or MSC-EVs were applied immediately after reperfusion (created

with https://BioRender.com). (**B**) Neurological deficits assessed by the Clark score at 24, 48, and 72 h post-MCAO. (**C**) Infarct volume and brain edema evaluated by cresyl violet staining, (**D**) neuronal injury in the ischemic striatum assessed by TUNEL/NeuN immunolabeling, (**E**) ICAM-1 expression on $CD31^+$ microvessels in the ischemic striatum, (**F**) density of brain-infiltrating $CD45^+$ leukocytes in the ischemic striatum, and (**G**) density of brain-infiltrating T cells or neutrophils in the ischemic striatum at 72 h post-MCAO. Representative cresyl violet stainings (in (**C**)) and immunohistochemistry images (in (**D**-**G**)) are shown. Data were compared by two-way repeated-measures ANOVA followed by Šidák's post hoc test (in (**B**)) or unpaired *t* test or Mann-Whitney U test, as appropriate (in (**C**-**G**)). No significant group differences were noted (n = 7–8 mice/group). Scale bars: 1 mm (in (**C**)), 50 µm (in (**D**, **G**)), 100 µm (in (**E**, **F**)).

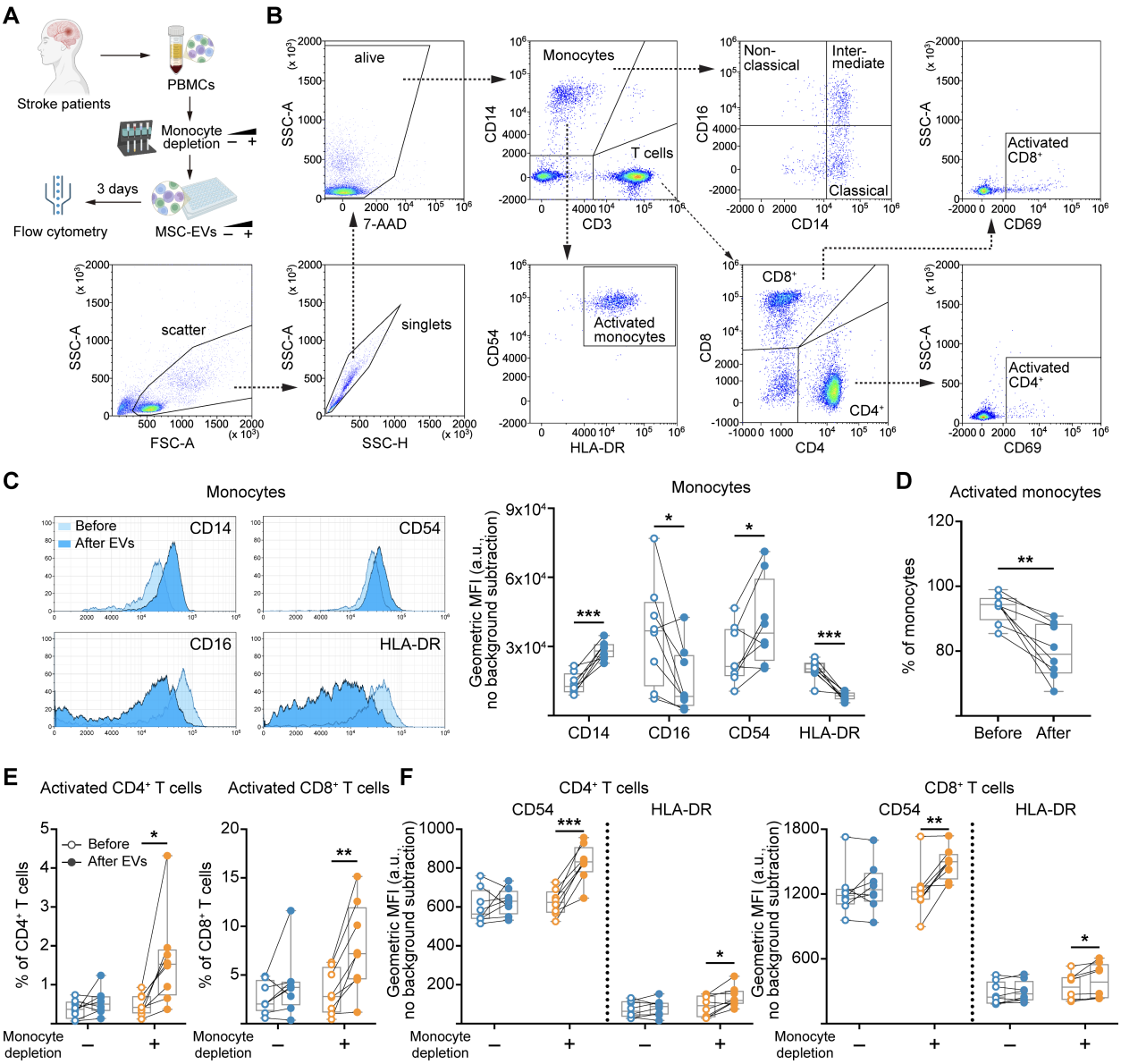

Figure 6. MSC-EVs induce phenotypic monocyte reprogramming while promoting CD4⁺ and CD8⁺ T cell activation in the absence of monocytes in peripheral blood mononuclear cells (PBMCs) obtained from acute ischemic stroke patients. (**A**) Experimental design: PBMCs were isolated from stroke patients 3–6 days after stroke onset. Intact or monocyte-depleted PBMCs were cultured for 3 days in the presence or absence of MSC-EVs, followed by flow cytometric analysis (created with https://BioRender.com). (**B**) Gating strategy for the analysis of PBMCs. (**C**) Representative histograms and corresponding quantification of CD14, CD16, CD54, and HLA-DR expression on monocytes. (**D**) Quantification of activated monocytes

(CD14$^+$ CD54$^+$ HLA-DR$^+$), (**E**) activated CD4$^+$ (CD3$^+$ CD4$^+$ CD69$^+$) and CD8$^+$ (CD3$^+$ CD8$^+$ CD69$^+$) T cells, and (**F**) CD54 and HLA-DR expression levels on CD4$^+$ and CD8$^+$ T cells in the presence or absence of monocytes, with or without MSC-EV treatment. Data were compared using paired *t* test. Paired *t* tests were performed on the raw geometric mean fluorescence intensity (MFI) values exported from Kaluza software without additional background subtraction or log transformation before statistical analysis. *p < 0.05, **p < 0.01, ***p < 0.001 (n = 8 patients; each pair represents an individual stroke patient).

Graphical abstract

